Journal of Ultrafine Grained and Nanostructured Materials
https://jufgnsm.ut.ac.ir
Vol. 56, No.2, December 2023, pp. 232-245
Print ISSN: 2423-6845 Online ISSN: 2423-6837
DOI: 10.22059/jufgnsm.2023.02.12

Synthesis of dual-phase face-centered cubic crystal structure in nanocrystalline AlCoCuFeNi high-entropy alloy

Elahe Mansouri [1], Hamid khorsand [1,*]

[1]Faculty of Materials Science and Engineering, K. N. Toosi University of Technology, No. 7, Pardis St., Mollasadra Av., Vanak Sq., Tehran, Iran.

Recieved: 16 September 2023; Accepted: 10 November 2023

**Corresponding author email: hkhorsand@kntu.ac.ir*

ABSTRACT

Nearly two decades have passed since the introduction of high entropy alloys, which can be synthesized using solid, liquid, or gas methods. This study focuses on the solid-state method of mechanical alloying to create high entropy alloy AlCoCuFeNi and examines the properties of the material at various stages of synthesis. The solid-state method of mechanical alloying was utilized in this research to synthesize a high entropy alloy, with samples taken at regular intervals of 10, 20, 30, 40, and 50 hours. X-ray diffraction (XRD) was used to characterize the alloys, with further XRD analysis performed to determine crystallite size and lattice strain. In this study, high entropy alloys were successfully synthesized as two-phase solid solutions with a dual-phase crystal (FCC) structure. The resulting alloy had a crystallite size of 8.4 nm and a residual strain of 1.7%. Elemental mapping image revealed that after 50 hours of mechanical alloying, all elements in the high entropy alloy were dissolved into each other with nearly identical atomic ratios, a finding confirmed by XRD analysis. The solid solution alloys synthesized in this research exhibited an intriguing phase separation phenomenon at the nano scale. The observation of dual phases with different lattice constants highlights the versatility of high entropy alloys and their potential for diverse applications

Keywords: *High entropy alloy, Mechanical Alloying, phase separation, powder metallurgy.*

1. Introduction

Pure metals rarely show suitable mechanical properties for structural applications. For this purpose, alloying elements are used to achieve the desired microstructure and an optimal combination of strength and toughness [1]. In 2004, a new example of an alloy design was proposed, which included the combination of several elements together to form an alloy. These multi-component alloys were designed by Yeh et al.[2] and were named High Entropy Alloys (HEAs), which indicated the high entropy of the random combination of elements in these alloys. The concept of high entropy introduces a new path for the development of advanced materials with unique properties that cannot be achieved by conventional alloys [3]. In normal alloys, there is always a dominant element in them, but in HEAs, none of the used elements are dominant, and in these alloys, each element is used almost equally, and a lot of configurational entropy is created in these alloys [2]. The type and number of constituent elements are effective factors in

determining the type of microstructure and properties of HEAs. This has caused these alloys to be used in many applications, such as tools[4], molds, mechanical parts, and furnace parts [5]. The high entropy of these alloys leads to the formation of FCC (face centered cubic) and BCC (body centered cubic) solutions instead of complex microstructures. Alloys containing elements with close atomic ratios have high state entropy. As a result, according to the Gibbs free energy formula, an increase in entropy causes ΔG to become more negative and, in fact more stable, makes it easier to form a solid solution [2,6]. HEAs are used as high-temperature alloys. Among their properties, high resistance against softening at high temperatures, low kinetic penetration, high resistance against fracture, high resistance against creep, and good compressive strength at room temperature can be mentioned [7]. HEAs typically exhibit a high melting point and retain strength at extremely elevated temperatures. In some cases, the strength of HEAs surpasses that of conventional superalloys. These unique properties make HEAs promising candidates for high-temperature applications, where they can offer superior mechanical performance compared to traditional alloys. The exceptional strength and thermal stability of HEAs have garnered significant attention in materials science and engineering, positioning them as potential alternatives to existing high-temperature structural materials [3].

Among different HEAs, the FeCoNiCuAl system has been studied a lot due to its unique features [8,9]. Various methods such as arc melting and casting [10,11], vacuum casting [12], Bridgman solidification [13], deposition with electric spark [14], and plasma spark sintering [15] have been used to make this alloy. This alloy shows a dual-phase FCC structure in all processing routes. The reason for using CoFeNiCuAl as a base for high entropy alloy is that based on dissolution conditions such as mixing enthalpy, atomic size, and electronegativity, Co, Cu, Fe, and Ni elements have good solubility. The CoFeNiCuAl system is associated with a combination of dual-phase crystal structures with excellent characteristics in hardness and compressive strength, which is considered as an excellent base in high entropy alloy[16]. Also, this alloy shows phase stability and unique mechanical properties under very high temperature and pressure conditions[17].

Generally, mechanical alloying steps have been investigated in several studies [18,19]. In the stage of "formation of equiaxed particles", welding and fracture happen successively at the same ratio. The last step is the random orientation of the particles. In the context of steady-state processing, the interlayer spacing becomes so refined that it is no longer discernible in SEM micrographs, and the size of the crystallites can be examined using XRD. This phenomenon is often observed when the crystal lattice becomes imperfect, leading to the broadening of X-ray diffraction peaks. The microstructure, which denotes the extent and quality of lattice imperfections, is a key factor in this process. Understanding the impact of these microstructural changes on material properties is essential for the comprehensive characterization of materials, particularly in the context of high strain rate deformation. Therefore, the precise analysis of microstructural parameters, such as interlayer spacing and crystallite size, is fundamental for gaining insights into the behavior of materials under various processing and loading conditions. The configurational entropy affects the rate of dissolution and speed of alloying. The optimal mechanical alloying time for single phase FCC FeNi systems is 20 hours, while for CoCrFeNi, CoCrFeMnNi, and CoFeNi, it is 15 hours[20]. Optimal grinding time has been studied to synthesize nanostructures[21-23], and some research has also been conducted for high entropy alloys [24,25]. Milling time may vary depending on the type, intensity, ball to powder ratio (BPR), and process temperature [26]. For high entropy alloys, process speed [27] and BPR [28] have been of interest to researchers. Additionally, changing the size of the ball increases the energy transferred through the ball to the powder[27]. Researchers were able to synthesize AlCuNiFeCr high entropy coating in the solid-state[28]. In another study, the optimum time of powder particle crushing was identified, which did not change the size of the particles over time[29]. The characteristics of mechanical alloying and the time of crystallite refinement have been fully described and studied, as reported by Mirzadeh and Zomardian [30].

1.1. Design of HEA

The properties of high entropy alloys can be significantly different from those of conventional alloys due to the high degree of compositional complexity. The design of high entropy alloys is therefore a critical aspect of their synthesis. One key principle in the design of HEAs is to ensure that the elements are alternated in the unit cell. This

is because the atomic radius of different elements can vary slightly, and if atoms of the same element are placed too close to each other in the unit cell, it can lead to unfavorable atomic packing and reduce the stability of the alloy. Therefore, it is essential to design HEAs in such a way that does not favor the placement of each atom in each position.

High entropy alloys with a single FCC phase are predicted to be ductile without high strength. [31] Researchers used AlCoCrFeNi2.1 EHEA to engineer an ultrafine dual microstructure and showed that the intentionally layered nature of the dual-phase composite improved the strength compared to previously reported methods. The as-prepared samples exhibited hierarchical structural heterogeneity due to phase separation and the improvement of mechanical properties observed during deformation is also attributed to an effect of the inhibition mechanism produced by the micro cracks itself [32- HEAs typically exhibit

35].

The phase separation and its mechanism in HEAs have not been thoroughly examined and discussed to date. A summary of multicomponent alloys, as presented in Table 1, demonstrates the occurrence of phase separation in the literature. Equiatomic Cu is a common component in these alloys. This prevalence is attributed, in part, to the positive mixing enthalpy Cu exhibits with many of the alloying elements in the system. It is noteworthy that while Ni seems to enhance miscibility in Cu-containing HEAs, this effect may be mitigated if the repulsion between Cu and the majority of the alloying elements is particularly strong.

Aluminum, nickel and copper powder have FCC phases, this partially predicts the final phase of the structure as FCC [41]. Based on the past research, when the atomic ratio of the elements in the composition of the HEAs AlCoCuFeNi is the same, the dominant phase is FCC[42]. Many studies have reported high entropy alloys without the presence of copper as a single phase, but the presence of the copper element due to the positive enthalpy and repulsion definitely causes the separation of the structure [43]. The positive mixing enthalpy of copper leads to phase separation and, in most cases, formation of dual-phase HEAs. Accordingly, the engineering of the final phases of the alloy as well as the complexity of the chemical composition is the first effective step in choosing the elements of a multicomponent system[44].

1.2. Theory of HEA

The energy stability of a system is higher in cases where the mixing enthalpy is negative. Therefore, elements with positive mixing enthalpy tend to separate more readily. Moreover, a higher temperature is required to prevent phase separation in the liquid state. However, even if phase separation does not occur in the liquid state, it can occur during cooling[40]. The researchers have suggested that separated layers or phases are associated with a large miscibility gap and that even the high entropy of equimolar mixtures may not be sufficient to pro-

Table 1- High entropy alloys with copper element

No	System	Ref.
1	Cr-Cu-Fe-Mo-Ni	[32]
2	Ag-Al-Co-Cr-Cu-Fe-Ni	[36]
3	Ag-Al-Co-Cr-Cu-Ni	[37]
4	Al0.5-Co-Cr-Cu-Fe-V, Co-Cr-Cu-Fe, Co-Cr-Cu-Fe-Ni-Nb, Co-Cr-Cu-Fe-Ti-V	[38]
5	Co-Cr-Cu-Fe-Mo-Ni	[39]
6	Co-Cr-Cu-Mn, Co-Cr-Cu-Mn-V Co-Cr-Cu-V	[40]

Table 2- Weight percentage of powders used.

mote effective mixing between elements. In such cases, the multicomponent system is more stable in segregation[36]. Until now, researchers believed that heat treatment causes spinodal decomposition of the solid state, which affects magnetic resistance. This phenomenon can be considered either positive or negative. The selection of elements that lead to alloy separation is one of the key factors in the design of high entropy alloys. Therefore, studying other methods, such as the liquid state or cooling rate, may provide a microstructure with complex properties[38].

Based on previous studies[32], HEAs exhibit a variety of exceptional characteristics, primarily attributed to their capacity to create solid solutions rather than intermetallic compounds. The development and stability of solid solution phases are influenced by numerous factors. These factors include the atomic size difference, mixing enthalpy, and mixing entropy, all of which must be satisfied for the formation of solid solution phases in high-entropy alloys. This distinguishes them from bulk metallic glasses, where the atomic size difference is a significant point of differentiation. Additionally, the presence of equilibrium intermetallic phases in high-entropy alloys can be predicted using a simple thermodynamic criterion, which is a crucial aspect of understanding their phase stability and properties.

These factors contribute to the unique properties of HEAs, which include a higher degree of fracture resistance, tensile strength, and corrosion and oxidation resistance compared to conventional alloys.

The stability of high-entropy alloy (HEA) systems is governed by the disparity in Gibbs free energy, which is closely linked to entropy and enthalpy. The substantial configurational entropy of HEA contributes to its stable structure, while the nearly zero mixing enthalpy minimizes resistance to solid-solution phase formation. The subsequent section will discuss these two thermodynamic parameters. The variance in Gibbs free energy (ΔG) is a fundamental factor in thermodynamics for determining phases in HEAs.

$$\Delta G_{Mix} = \Delta H_{mix} - T\Delta S_{mix} \quad (1)$$

The changes in mixing entropy and enthalpy are denoted by ΔSmix and ΔHmix, respectively, while T represents the absolute temperature. The solid solution system in high-entropy alloys (HEAs) can be viewed as an ideal solid solution with low mixing enthalpy and non-configurational mixing entropy. The variation in Gibbs free energy is mainly influenced by configurational entropy, which affects phase stability [47].

The ΔS_{mix} can be defined via Boltzmann's hypothesis as follows:

$$\Delta S_{mix} = -R \sum_{i=1}^{n} C_i \, Ln C_i \quad (2)$$

The symbol R represents the gas constant, and C_i represents the mole percent of the component, where $\sum_{i=1}^{n} C=1$. As per Equation (2), the mixing entropy reaches its maximum when the molar percentage of the alloy is equal. Simultaneously, the Gibbs free energy difference is at its lowest, leading to the formation of a stable structure. In equiatomic multicomponent high entropy alloys, the enthalpy and non-configurational entropy play a more crucial role than the configurational entropy in terms of phase stability. Moreover, the mixing entropy of HEAs with suitable components can approach a maximum value with minimal variation [47,32]. Considering the mixing enthalpy is essential.

Another key characteristic parameter is the mixing enthalpy, which can be expressed as follows:

$$\Delta H_{mix} = \sum_{i=1, i\neq j}^{n} \Omega_{ij} \, C_i C_j \quad (3)$$

$$\Omega = \frac{T_{m\Delta S_{mix}}}{\Delta H_{mix}} \quad (4)$$

where C_i or C_j denotes the atomic percentage of the ith or jth component. Ω_{ij}= ($4\Delta H_{AB}^{mix}$). where ΔH_{AB}^{mix} is the mixing enthalpy for the binary liquid AB alloys. As the ΔH_{AB}^{mix} becomes more positive, the elements in HEAs tend to separate more easily, while more negative ΔH_{AB}^{mix} values favor the formation of intermetallic compounds. T_m represents the average melting point of all constituent elements [32]. The ratio Ω of $T_m\Delta S_{mix}$ and $|\Delta H_{mix}|$ is commonly used to assess the solid-solution formation ability, which is more accurate than individual entropy or enthalpy considerations.

The lattice structure of High Entropy Alloys (HEAs) typically undergoes significant distortion, distinguishing it from the relatively uniform lattice structure found in pure metals. This distortion arises when the constituent elements of HEAs maintain their original size but are forced into the lattice. As a result, the lattice structure of HEAs differs substantially from that of pure metals. The high entro-

py effect of HEAs plays a vital role in stabilizing the phase structure through lattice distortion, ensuring that the distortion is sufficient to maintain phase structure stability. To quantify this distortion, the atomic size difference (δ) is commonly expressed using the following equation:

$$\delta=\sqrt{\sum_{i=1}^{n} c_i \left(1-\frac{r_i}{\bar{r}}\right)^2}\ ,\bar{r}=\sum_{i=1}^{n} c_i\, r_i \qquad (5)$$

here, C_i and r_i are the atomic percentage and the atomic radius of the ith atom, respectively.

A quantitative criterion for the formation of a simple solid solution in HEAs was proposed in a recent review paper [47], which includes the following criteria: $-10 \le \Delta H_{mix} \le 5$ kJ/mol , $\Delta S_{mix} \le 13.38$ J/(mol.k) , and $\delta \le 4\%$. However, the observations of this research contradict a group of researchers who suggested that a positive mixing enthalpy would be expected if there is a large difference in atomic radius but a small difference in electronegativity.

The number of valence electrons is closely associated with the chemical activity of alloys, influencing bonding and structure stacking. While not entirely precise in predicting structure, the Valence Electron Concentration (VEC) is a key parameter for phase stability at room temperature and is generally essential to calculate. The VEC, defined as the sum of the atomic percentages of the valence electrons of each element, has been found to significantly impact the phase stability of alloys. Understanding the influence of VEC on phase stability is crucial in the design of alloys and the regulation of the mechanical properties of HEAs. The VEC is defined as[45,46]:

$$\mathrm{VEC}=\sum_{i=1}^{n} C_i\, VEC_i \qquad (6)$$

where C_i is the atomic percentage of ith element, VEC_i is the VEC of ith element. The phase development of solid solutions of the FCC or BCC type can be quantitatively anticipated using the Valence Electron Concentration (VEC). Stable phases are FCC when the VEC value exceeds 8, BCC when it is less than 6.87, and a coexistence of mixed FCC and BCC phases when the value falls between 6.87 and 8. This understanding of the effect of VEC on phase stability is crucial for alloy design of HEAs.

Nonetheless, the results of this study confirm that an increased probability of separation occurs even in single-phase systems when the VEC falls within a range of 8.09-8.44 and δ is between 3.39 and 4.25 [32]. Additionally, VEC has an impact on the arrangement of atoms [46].

In this research, the selection of elements for the high entropy alloy was based on the consideration of both electronegativity and atomic radius. Iron, aluminum, copper, cobalt, and nickel were chosen as the constituent elements for their favorable properties and their compatibility with the principle of atomic alternation in the unit cell.

According to the information stated in the introduction, in past research, the combination of iron, nickel, cobalt, copper and aluminum has been investigated and synthesized. In this research, we have studied and investigated this high entropy compound using mechanical (wet) alloying. We have also checked the elemental mapping of AlCoCuFeNi image and the formation of phases by XRD. The main objective of the present work is to fabricate a nanocrystalline dual phase FCC HEA. Considering this purpose, elements with FCC structures such as Co, Ni, and Cu were selected.

The synthesis of nanocrystalline HEAs offers advantages due to the superior combined mechanical and functional properties achieved through

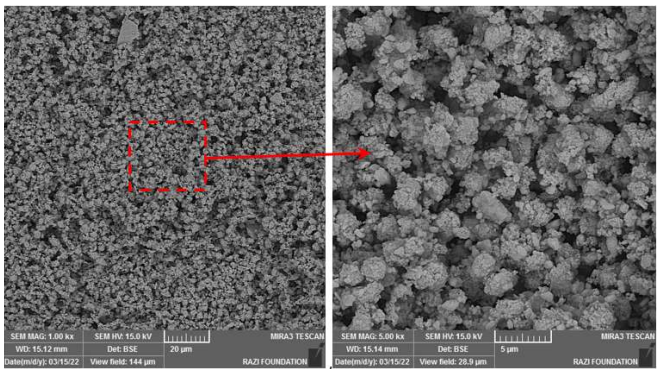

Fig. 1- SEM image of the morphology of AlCoCuFeNi powder particles.

solid-solution strengthening and grain-boundary strengthening. Mechanical alloying is superior to other nanocrystalline material synthesis methods due to its shorter processing time and lower energy consumption making it a more efficient and cost-effective technique. In our research, we have utilized the mechanical alloying method for the synthesis of nanocrystalline AlCoCuFeNi HEAs.

2. Experimental details

The high entropy alloy AlCoCuFeNi was synthesized using powders of Al, Co, Cu, Fe and Ni with a purity of over 99 % and a size of less than 50 μm. Initial mixing was performed using a simple mixer, followed by sampling and XRD analysis. Mechanical alloying was initiated with a ball to powder ratio of 1:10, using 30 g of powder in a 300 cc mechanical alloying chamber with stainless steel balls. The balls were decontaminated using an electrolysis machine for 10 minutes. To prevent oxidation of the powders, acetone with a weight of 30 grams (equal to the powder) was used as the liquid process control agent (PCA). The innovation of using a liquid PCA was to prevent oxidation the powders, ball, and mixed PCA were then milled in a high-energy ball mill at 500 rpm, with sampling performed every 10 hours.

Figure 1 displays the spherical morphology of the raw material powder in the state of simple mixing, as observed through SEM imaging. These findings highlight the precision and care taken in the synthesis process, which can impact the resulting alloy's properties and performance.

Philips XRD X'pert MPD diffractometer (Cu Kα radiation, 40 kV and 30 mA) was used to investigate the structural changes, constituent phases, grain size, and lattice strain. Cu kα X-rays with a wavelength of 1.542 Å, a step time of 1s, a step size of 0.05 degrees, and an angle range of 20 to 80 degrees were selected to perform the test. Also, XPERT PLUS software was used to check constituent phases and Scherer's relation was used to calculate crystallite size. The Scherrer equation can be written as the following equation:

$$t = \frac{K\,\lambda}{B\cos\theta} \tag{7}$$

The Scherrer constant, denoted as K, is a parameter that characterizes the shape of particles. It is commonly assigned a value of 0.9. In the context of X-ray diffraction, the Scherrer equation is utilized to determine the average crystallite size in a material. The equation incorporates the wavelength of the X-ray beam (λ), the full width at half maximum (FWHM) of the peak (β), and the Bragg angle (θ). This fundamental equation is instrumental in the analysis of microstructural parameters from X-ray diffraction peak broadening, providing valuable insights into the characteristics of materials at the nanoscale.

A Philips XL30 series scanning electron microscope (SEM) was used to investigate and observe the effect of mechanical alloying steps on the morphology and particle size of the produced alloy powder. The elemental distribution of the samples was also determined by energy dispersive spectroscopy (EDS).

3. Results and discussion

As mentioned, this research focused on the synthesis of dual-phase high entropy alloy. Mechanical alloying synthesis method was chosen to achieve this goal. Elements with the minimum difference in atomic radii were selected, which, according to the laws of high entropy alloys, have a high probability of forming an HEA structure.

The Miedema's model states that the enthalpy of solid solution formation comprises three parameters: the enthalpy from atom mixing, the mismatch due to differences in atom size, and the variance in valence electrons of the solvent and solute atoms' crystalline structure. For high entropy alloys, calculating the change in chemical enthalpy or mixing is essential, as presented in Table 2, which details the mixing enthalpy in this research [48,49].

Enthalpy and entropy are vital factors in predicting the formation of high entropy alloys. However, given the complexity of these alloys, additional parameters such as δ, Ω, and VEC have been proposed to more accurately characterize and forecast the final product. Table 3 shows the calculations of thermodynamic parameters using equations 1 to 6.

In this particular research, the samples were taken every 10 hours to observe the stages of mechanical alloying. The electron microscope images in Figure 2 (a) provide a visual representation of the microstructural changes that occurred during the alloying process. These images are important for understanding the progress of the alloying process.

As shown in Figure 2 (a), after 10 hours of mechanical alloying, plastic deformation and cold welding of powder particles occurred, resulting in the formation of crystallites with a size of 9.25 nm. Increasing the milling time to 20 hours led to an

Table -2 Enthalpy of the elements of this research [48]

ΔH_{ij}	Fe	Co	Ni	Cu	Al
Fe	0	-1	-2	13	-11
Co	0	0	0	6	-19
Ni	0	0	0	4	-22
Cu	0	0	0	0	-1
Al	0	0	0	0	0

Table 3- Calculation of thermodynamic parameters AlCoCuFeNi HEA

parameter	$\Delta S\left(\frac{kJ}{mol.K}\right)$	$\Delta H\left(\frac{kJ}{mol}\right)$	δ (%)	Ω	VEC	$\Delta G\left(\frac{kJ}{mol}\right)$
AlCoCuFeNi	13.38	-5.28	3.65	3.85	8.2	-18.66

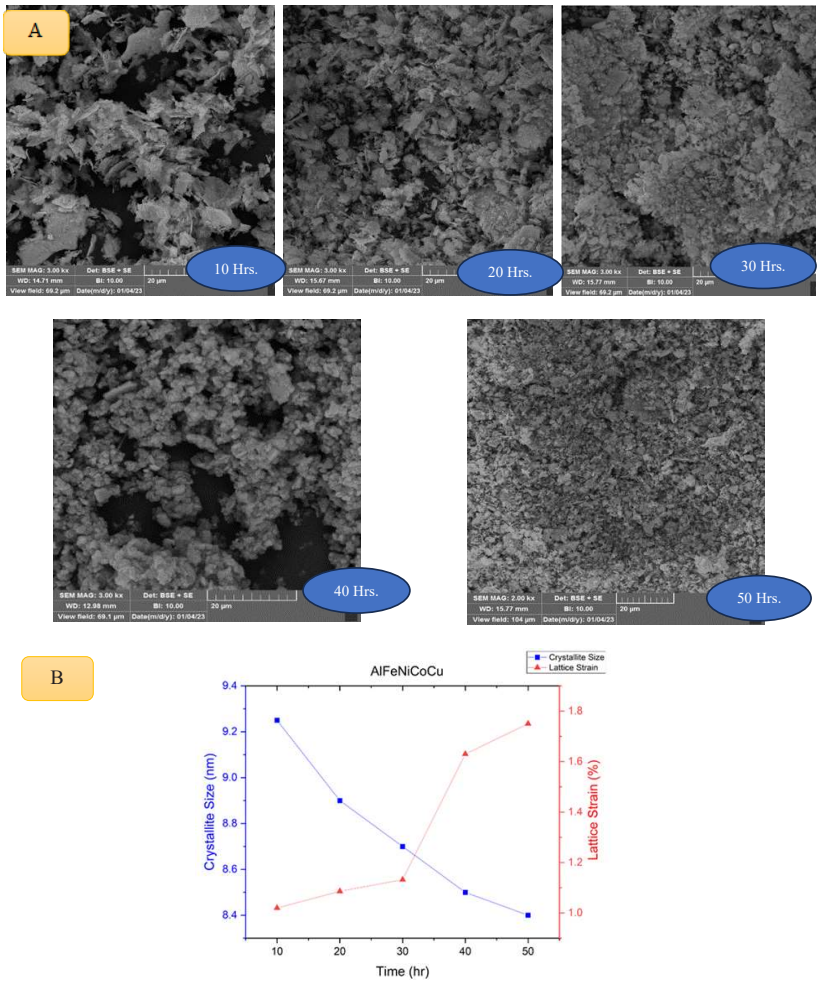

Fig. 2- SEM images at different times of mechanical alloying at 10, 20, 30, 40, and 50 hours, (b) The effect of milling time on lattice strain and crystallite size of AlCoCuFeNi powder.

increase in the density of dislocations, resulting in greater hardness and facilitated failure of the particles. By increasing the time of milling process up to 20 hours, the fracture mechanism gradually overcame the cold-welding mechanism, and the particle size decreased to 8.9 nm. After 30 hours of milling, the particles were crushed with a smaller slope, in this stage, it was evident that cold welding had a more pronounced effect compared to the previous, resulting in a decrease in crystallite size distribution to 8.5 nm. Further reduction in crystal size was observed after 50 hours of milling, reaching 8.4 nm. Figure 2 (b) illustrates the relationship between crystallite size distribution and lattice strain over the course of mechanical alloying time.

The uniform distribution of elements in the image is shown in Figure 3 the elemental mapping after 50 hours mechanical alloying.

Mechanical alloying is associated with an increase in the strain of the structure, which is calculated and plotted in Figure 4. In metallurgical and crystallographic literature, the term "strain" is

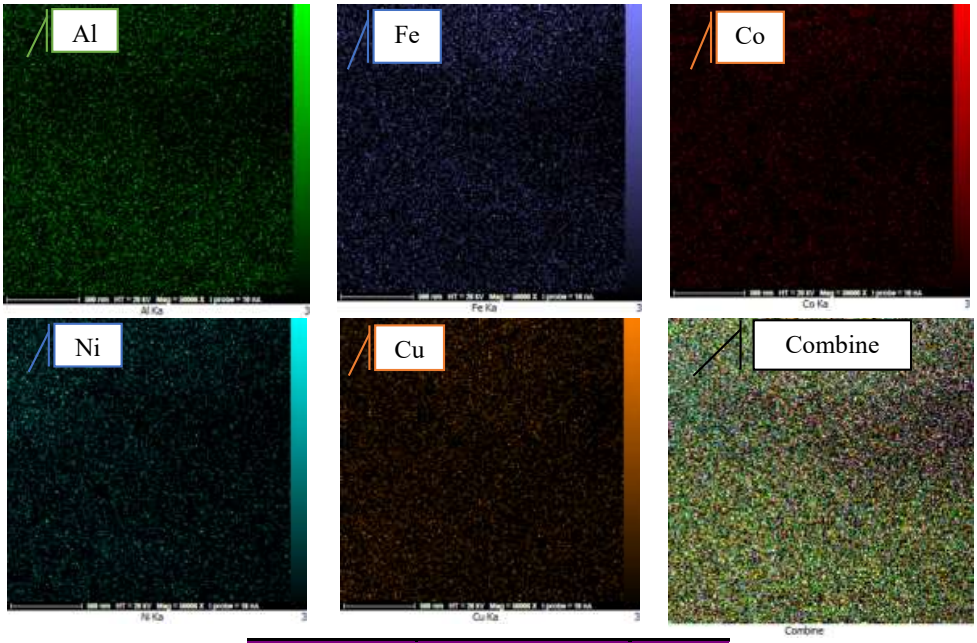

Elt	W%	A%
Al	15.5	17.3
Fe	21.0	21.8
Co	19.3	19.0
Ni	20.7	20.5
Cu	23.3	21.2

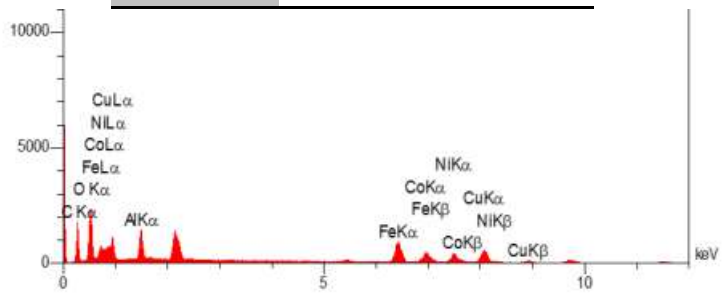

Fig. 3- Elemental mapping of AlCoCuFeNi image after 50 hours of mechanical alloying.

frequently employed to describe various structural distortions within materials. It's essential to clarify these distinctions to avoid confusion, particularly in the context of HEAs, where past literature has sometimes attributed strains incorrectly.

Figure 4 (a) represents the material in an unstrained state. The blue color indicates the unstrained condition, while the red dashed line illustrates peak displacement and its effect on peak appearance. There are generally three recognized categories of strain, classified based on either the cause of displacement or the length scale over which the strain operates. It is important to understand how each type of strain manifests in experimental data, as this understanding also applies to how each type affects diffraction data, which is a widely used method for analyzing strains. These diagrams aim to elucidate the impact of various strain types on the observed diffraction data: Figure 4 (b) shows that macroscopic strains affect large regions of the material, often spanning the entire sample or component. These strains result from bulk applied stresses, which cause uniform deformation of all crystals within the material along a single direction. In diffraction data, reflections aligned with the plane normal parallel to the applied stress exhibit changes in interplanar spacings, either increasing or decreasing in response to the stress. In Figure 4 (C), Type c strains act on a smaller scale than Type b strains and vary within the material's microstructure. They arise due to crystallographic anisotropy, which leads to non-uniform changes in interplanar spacings in diffraction patterns. Type e strains in Figure 4 (e) operate at an even smaller length scale, within individual crystals, and result from localized disruptions in the long-range lattice structure caused by stress fields around crystal defects, such as dislocations or atomic interface discontinuities. These disruptions cause slight changes in interplanar spacings, leading to broader diffraction peaks when a wider angular range results in constructive interference. The three categories of strains discussed earlier encompass a broad range of strains, but atomic-level displacements due to alloying effects require distinct consideration. This is particularly crucial in HEAs, where a highly distorted lattice structure plays a central role. When a secondary atom with a different atomic radius is incorporated into a host lattice, it induces local distortions that displace neighboring host atoms due to size mismatches. In cases of substitutional incorporation, as seen in HEAs, these displacements are

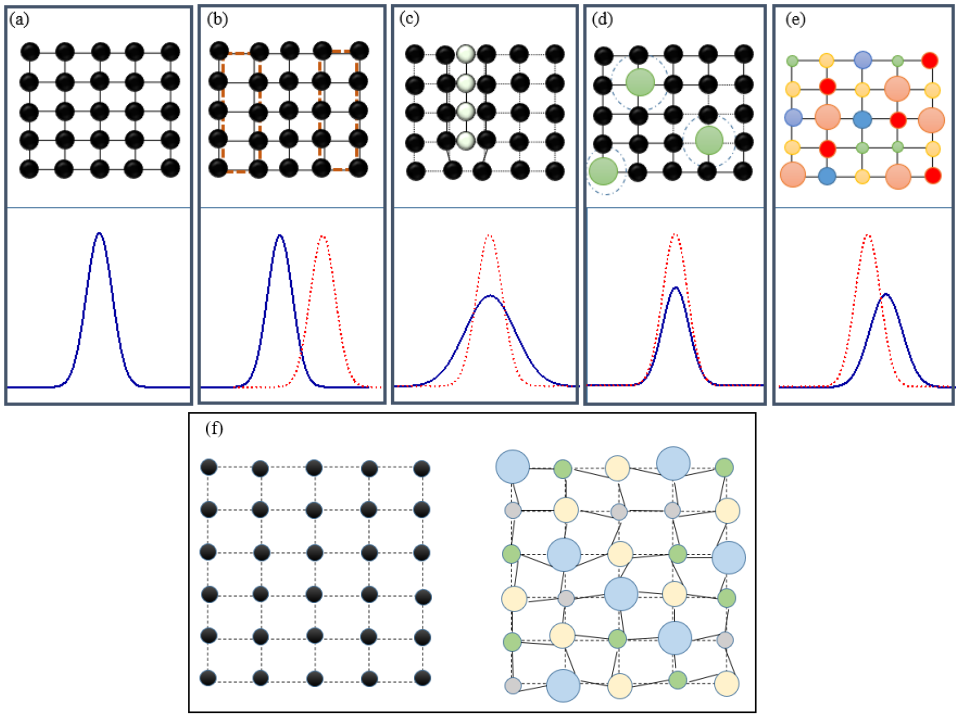

Fig. 4- a, b, c, d, and e Comparison of strain in crystal lattices. (f) Compare ideal monoatomic material and high entropy alloys.

isotropic. To clarify, we refer to the static displacement of an atom from its ideal position as local lattice strain, which can be considered an additional strain type, similar to Type e. It is important to note that in any real crystal at a given temperature, constituent atoms experience displacements from their ideal positions due to thermal oscillations. In defect-free crystals, these oscillations center around the ideal position, with the average atom position aligning over time. These dynamic displacements, resulting from thermal motion, are not considered a form of local lattice strain. However, in crystals with static displacements, such as solid solutions, thermal oscillations occur around the displaced location rather than the ideal position, resulting in instantaneous atom locations being a combination of static and dynamic displacements.

Figure 4 (f) schematically compares the high entropy alloy with a normal crystalline structure. The presence of strain in the network structure is not favorable in terms of energy and makes the solid solution unstable. According to the Hume-Routery law, there is a direct relationship between the solubility of the solid phase and the local strain in the network. In this way, if the difference in atomic radius in binary solutions is more than 15%, the solubility decreases. Accordingly, we find that the difference in atomic radius plays a decisive role in the local strain and solubility of the solid phase. Based on this, it is predicted that there is a certain limit for increasing the network strain, beyond which the system becomes thermodynamically unstable and decomposes. But no answer was found to calculate this range. Substitution of elements with a larger atomic size or larger radius causes the structure to expand. In binary alloys, the expansion of the unit cell network structure is described and calculated by Vegard's law. In general, it is found that the substitution of larger elemental species results in a wider structured network. According to Vegard's law, the lattice parameter has a direct relationship with the number of alloying elements. However, this rule is violated in the case of high entropy alloys, and it is not possible to find a linear dependence between the lattice parameter and the percentage of alloy elements in multicomponent systems[50].

The difference in the ionic radius of the main and impurity ion means that if the ionic radius of the impurity ion is greater than the main ion, the lattice constant increases and if the ionic radius of the impurity ion is smaller than the parent ion, the lattice constant decreases. Based on the factor, generally in solid solutions, Vegard's law is used to calculate the lattice constant.

The pattern of phase changes in the AlCoCuFeNi system during the mechanical alloying process from zero to 50 hours using X-ray diffraction analysis is shown in Figure 5. The diffraction patterns of all pure elements can be seen in zero hour. With increasing milling time, peak intensities sharply decreased after 10h of the milling process, indicating the beginning of dissolution. After 10h, the Al peak completely disappeared and the intensity of the Co and Ni peaks decreased more sharply than that of the Fe and Cu peaks. Al dissolves faster than other elements, which means that Al has the highest alloying rate compared to other elements in the system, which can be due to the lower melting point / higher diffusion coefficient of Al.

After 20 hours of milling, the Co peaks almost disappeared, but the Fe and Ni peaks were still visible, indicating a low alloying rate between Fe and Ni, according to research by Chen et al.[51], this can be due to the high melting point/lower penetration coefficient of these elements. These studies have shown that higher melting temperatures reduce the amount of alloying because an element with a higher melting point has a higher bond strength and therefore a lower penetration coefficient. From a mechanical point of view, an element with a lower melting point usually has a lower hardness, thus has better flexibility (hammering) to help disperse. This means that in the initial stage, elements with higher malleability such as Al can penetrate more rapidly into other elements and the solution phase. Due to the melting point of Co (1495 °C) and Ni (1455 °C) According to the melting point of nickel, it is expected that during mechanical alloying process, its alloying speed is higher than cobalt, but because cobalt has an hcp structure and has less slip systems, cobalt is more brittle. Therefore, the melting point is the primary factor to determine the alloying speed of an element, and secondary factor such as the crystal structure is more important for elements with similar melting points [52].

By increasing the milling time up to 30 hours, the very small peaks were removed and no other peaks were recognizable except the three main peaks of the FCC structures. The lattice parameters of this system were determined after mechanical alloying for HEA. As the milling time increased from 30 hours to 50 hours, no change was observed in the XRD patterns except flattening of the main

peak. During the milling process, a decrease in intensity, peak flattening, and subsequent disappearance may be the result of factors such as shrinking of crystallite size, lattice strain, and reduced crystallinity [53].

Dual phases FCC1 and FCC2 were observed in the synthesized alloy[39], as shown in Figure 5.

One of the important things in mechanical alloying is changes of the lattice constant due to this process. In Table 4 lattice constant in AlCoCuFeNi was calculated. After 50 hours mechanical alloying, the interplanar distances for the FCC1 phase have been meticulously determined, and they perfectly correspond to the reflections emanating from these specific planes (111), (200), and (220) were 2.076, 1.799, and 1.468 Å, respectively. In the same way the lattice parameter of the FCC1 phase was found to be 3.78 Å. Interplane distances calculated after 50 hours of mechanical alloying in the FCC2 phase attributed to reflections from (111), (200), and (311) planes, were 2.912, 2.510, and 1.596 Å, respectively. Also, the FCC2 phase lattice parameter was equal to 5.12 Å.

Lattice distortion in HEAs is a fundamental issue that has not been studied by many researchers. Mechanical alloying of elements that have different sizes creates a residual strain field with atomic scale fluctuations caused by the difference in atomic size and the mismatch of the Elastic modulus of primary elements (before alloying). The residual strain field includes two volume and shear components. It can be considered that the average value of the residual strain can be neglected and thus the network constant is close to each other for both networks. The size of the residual strain fluctuation is a measure of the lattice strain, which is also attributed to

Table 4- Lattice constant in AlCoCuFeNi

Phase	*Peak Num.*	*d-Spacing (Å)*	*Pos. (2θ)*	*h*	*k*	*l*	*Lattice Parameter (Å)*
FCC 1	1	2.079	43.56	1	1	1	3.78
	2	1.799	50.71	2	0	0	
	3	1.468	63.50	2	2	0	
FCC 2	1	2.912	30.69	1	1	1	5.12
	2	2.510	35.76	2	0	0	
	3	1.596	57.74	3	1	1	

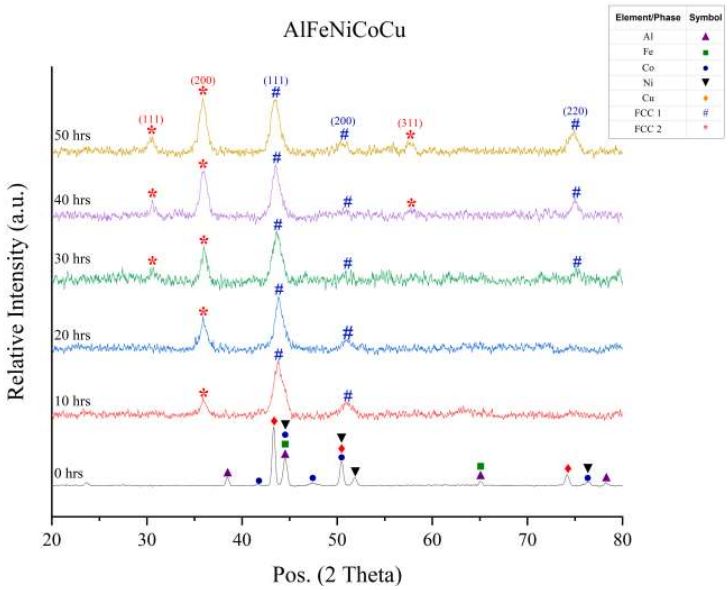

Fig. 5- X-ray diffraction pattern at different times of mechanical alloying for AlCoCuFeNi system.

Poisson's ratio of an alloy in addition to the difference in atom size [54].

These parameters are shown in Table 5. By carefully examining the position of the main peak in the X-ray diffraction pattern for different milling hours, it can be seen that the main peak has been moved to smaller angles. With increasing mechanical alloying time, the amount of this displacement increased. According to Bragg's law, moving the peaks to smaller angles indicates an increase in the distance between the plates and thus the lattice parameter [46,55].

Therefore, the lattice parameter has increased over time. The lattice parameters of the Fe-Co-Ni-Cu-Al system during the MA were calculated from the XRD patterns. According to Figure 5, it seems that with the penetration of Ni and Al elements, the HEA structure stabilizes towards a structure with a larger lattice parameter.

Finally, the presence of contaminants during mechanical alloying is one of the main problems of this method. Although complete control of pollution is impossible during the MA process, some suggestions can help to minimize the formation of unwanted contaminants. High purity powders and controlled atmosphere can be used to control pollution.On the other hand, the formation of a layer of powder on the balls, in this process, can prevent the entry of impurities and pollution, which can be controlled by choosing the right resting time[56]. In the present study, we tried to follow the above suggestions. For this purpose, high-purity primary powders and high-quality steel cups and balls were used for the MA process. In addition, light and short mills for Co-Fe-Ni-Cu-Al-Mn powders were done before the MA process. This resulted in the formation of a thin coating on the wall of the cup and balls, which further restricted the entry of the Fe element into the milled powders.

4. Conclusions

This study aimed to synthesize a high entropy alloy AlCoCuFeNi using mechanical alloying and investigate the thermodynamic phase stability of HEAs during the process. In summary, the study includes the following results:

1- Nanocrystalline AlCoCuFeNi HEA powder was successfully synthesized using mechanical alloying.

2- Analysis of the resulting powder using X-ray diffraction and scanning electron microscopy at different time intervals confirmed the formation of HEA after 50 hours of MA.

3- The synthesized powder after 50 hours of mechanical alloying has a crystallite size of 8.4 nm and a residual strain of 1.7%.

4- Thermodynamic calculations predicted the formation of two phases in the final alloy, which was confirmed by experimental data.

5- The presence of the copper element, due to the positive mixing enthalpy, led to a dual phase structure, highlighting the potential of the chemical composition's complexity in the design of high-entropy alloys.

Table 5- Burger's vector, lattice constant, Poison's ratio, and Crystal structure for the constituent elements in the AlCoCuFeNi system[55]

Element	Burger's Vector (Å)	Lattice Constant (Å)	Poison's Ratio	Crystal Structure
Fe	2.48	2.86	0.29	BCC
Co	2.48	2.50	0.32	HCP
Ni	2.48	3.52	0.31	FCC
Cu	2.55	3.61	0.34	FCC
Al	2.86	4.04	0.35	FCC

References

1. Ghanbariha M, Farvizi M, Ebadzadeh T, Alizadeh Samiyan A. Effect of ZrO2 particles on the nanomechanical properties and wear behavior of AlCoCrFeNi–ZrO2 high entropy alloy composites. Wear. 2021;484-485:204032.

2. Ye YF, Wang Q, Lu J, Liu CT, Yang Y. High-entropy alloy: challenges and prospects. Materials Today. 2016;19(6):349-62.

3. Zhang Y, Zuo TT, Tang Z, Gao MC, Dahmen KA, Liaw PK, Lu ZP. Microstructures and properties of high-entropy alloys. Progress in Materials Science. 2014;61:1-93. Zhang Y, Zuo TT, Tang Z, Gao MC, Dahmen KA, Liaw PK, Lu ZP. Microstructures and properties of high-entropy alloys. Progress in Materials Science. 2014;61:1-93.

4. Holmström E, Lizárraga R, Linder D, Salmasi A, Wang W, Ka-

plan B, et al. High entropy alloys: Substituting for cobalt in cutting edge technology. Applied Materials Today. 2018;12:322-9.
5. Ren B, Liu ZX, Li DM, Shi L, Cai B, Wang MX. Effect of elemental interaction on microstructure of CuCrFeNiMn high entropy alloy system. Journal of Alloys and Compounds. 2010;493(1-2):148-53.
6. Zhang H, Zhang L, Liu X, Chen Q, Xu Y. Effect of Zr Addition on the Microstructure and Mechanical Properties of CoCrFeNiMn High-Entropy Alloy Synthesized by Spark Plasma Sintering. Entropy (Basel). 2018;20(11):810.
7. Chikumba S, Rao VV. High entropy alloys: development and applications. InProceedings of the 7th International Conference on Latest Trends in Engineering & Technology (ICLTET'2015) 2015 Nov 26 (pp. 1-5).
8. Z. Wu, M. C. Troparevsky, Y. F. Gao, J. R. Morris, G. M. Stocks, and H. Bei, "Phase stability, physical properties and strengthening mechanisms of concentrated solid solution alloys," Curr. Opin. Solid State Mater. Sci., vol. 21, no. 5, pp. 267–284, 2017.
9. Feng H, Li H-B, Dai J, Han Y, Qu J-D, Jiang Z-H, et al. Why CoCrFeMnNi HEA could not passivate in chloride solution? – A novel strategy to significantly improve corrosion resistance of CoCrFeMnNi HEA by N-alloying. Corrosion Science. 2022;204:110396.
10. Wang FJ, Zhang Y. Effect of Co addition on crystal structure and mechanical properties of Ti0.5CrFeNiAlCo high entropy alloy. Materials Science and Engineering: A. 2008;496(1-2):214-6.
11. Manzoni A, Daoud H, Völkl R, Glatzel U, Wanderka N. Phase separation in equiatomic AlCoCrFeNi high-entropy alloy. Ultramicroscopy. 2013;132:212-5.
12. Qiao JW, Ma SG, Huang EW, Chuang CP, Liaw PK, Zhang Y. Microstructural Characteristics and Mechanical Behaviors of AlCoCrFeNi High-Entropy Alloys at Ambient and Cryogenic Temperatures. Materials Science Forum. 2011;688:419-25.
13. Zhang Y, Ma SG, Qiao JW. Morphology Transition from Dendrites to Equiaxed Grains for AlCoCrFeNi High-Entropy Alloys by Copper Mold Casting and Bridgman Solidification. Metallurgical and Materials Transactions A. 2011;43(8):2625-30.
14. Li QH, Yue TM, Guo ZN, Lin X. Microstructure and Corrosion Properties of AlCoCrFeNi High Entropy Alloy Coatings Deposited on AISI 1045 Steel by the Electrospark Process. Metallurgical and Materials Transactions A. 2012;44(4):1767-78.
15. Shahbazkhan A, Sabet H, Abbasi M. Investigation of bonding strength and hot corrosion behavior of NiCoCrAlSi high entropy alloy applied on IN-738 superalloy by SPS method. Journal of Alloys and Compounds. 2022;911:164997.
16. Yang F, Wang J, Zhang Y, Wu Z, Zhang Z, Zhao F, et al. Recent progress on the development of high entropy alloys (HEAs) for solid hydrogen storage: A review. International Journal of Hydrogen Energy. 2022;47(21):11236-49.
17. Ocak BC, Goller G. Investigation the effect of FeNiCoCrMo HEA addition on properties of B4C ceramic prepared by spark plasma sintering. Journal of the European Ceramic Society. 2021;41(13):6290-301.
18. Peng YB, Zhang W, Mei XL, Wang HJ, Zhang MY, Wang L, et al. Microstructures and mechanical properties of FeCoCrNi-Mo High entropy alloys prepared by spark plasma sintering and vacuum hot-pressed sintering. Materials Today Communications. 2020;24:101009.
19. Tian L, Fu M, Xiong W. Microstructural Evolution of AlCoCrFeNiSi High-Entropy Alloy Powder during Mechanical Alloying and Its Coating Performance. Materials (Basel). 2018;11(2):320.
20. Vaidya M, Muralikrishna GM, Murty BS. High-entropy alloys by mechanical alloying: A review. Journal of Materials Research. 2019;34(5):664-86.
21. Amiri Talischi L, Samadi A. Structural characterization and ordering transformation of mechanically alloyed nanocrystalline Fe-28Al powder. Journal of Ultrafine Grained and Nanostructured Materials. 2016 Dec 1;49(2):112-9.
22. Shahsavari E, Zamani C, Ahmadi Dermeni H, Hadian AM, Hadian A. Cryomilling-Assisted Synthesis of Nanostructured Silicon. Journal of Ultrafine Grained and Nanostructured Materials. 2020 Dec 28;53(2):158-65.
23. Haghighat-Shishavan S, Kashani Bozorg F. Nano-Crystalline Mg (2-x) MnxNi Compounds Synthesized by Mechanical Alloying: Microstructure and Electrochemistry. Journal of Ultrafine Grained and Nanostructured Materials. 2014 Jun 1;47(1):43-9.
24. Maulik O, Kumar D, Kumar S, Fabijanic DM, Kumar V. Structural evolution of spark plasma sintered AlFeCuCrMgx (x = 0, 0.5, 1, 1.7) high entropy alloys. Intermetallics. 2016;77:46-56.
25. Oleszak D, Antolak-Dudka A, Kulik T. High entropy multicomponent WMoNbZrV alloy processed by mechanical alloying. Materials Letters. 2018;232:160-2.
26. Enayati MH, Mohamed FA. Application of mechanical alloying/milling for synthesis of nanocrystalline and amorphous materials. International Materials Reviews. 2014;59(7):394-416.
27. Salemi F, Abbasi MH, Karimzadeh F. Synthesis and thermodynamic analysis of nanostructured CuNiCoZnAl high entropy alloy produced by mechanical alloying. Journal of Alloys and Compounds. 2016;685:278-86.
28. Chen C-L, Suprianto. Microstructure and mechanical properties of AlCuNiFeCr high entropy alloy coatings by mechanical alloying. Surface and Coatings Technology. 2020;386:125443.
29. Jain H, Shadangi Y, Shivam V, Chakravarty D, Mukhopadhyay NK, Kumar D. Phase evolution and mechanical properties of non-equiatomic Fe–Mn–Ni–Cr–Al–Si–C high entropy steel. Journal of Alloys and Compounds. 2020;834:155013.
30. Mirzadeh H, Zomorodian A. Ball milling criteria for producing nano intermetallic compounds. Materials Science and Technology. 2010;26(3):281-4.
31. Tang Z, Zhang S, Cai R, Zhou Q, Wang H. Designing High Entropy Alloys with Dual fcc and bcc Solid-Solution Phases: Structures and Mechanical Properties. Metallurgical and Materials Transactions A. 2019;50(4):1888-901.
32. eng Z, Liu N, Zhang SY, Wu PH, Wang XJ. Liquid-phase separation of immiscible CrCuxFeMoyNi high-entropy alloys. Materials Science and Technology. 2017;33(11):1352-9.
33. Liu K, Nene SS, Frank M, Sinha S, Mishra RS. Extremely high fatigue resistance in an ultrafine grained high entropy alloy. Applied Materials Today. 2019;15:525-30.
34. Shi P, Ren W, Zheng T, Ren Z, Hou X, Peng J, et al. Enhanced strength-ductility synergy in ultrafine-grained eutectic high-entropy alloys by inheriting microstructural lamellae. Nat Commun. 2019;10(1):489-.
35. Wang N, Wu B, Wu W, Li J, Ge C, Dong Y, et al. Microstructure and properties of aluminium-high entropy alloy composites fabricated by mechanical alloying and spark plasma sintering. Materials Today Communications. 2020;25:101366.
36. Munitz A, Kaufman MJ, Chandler JP, Kalaantari H, Abbaschian R. Melt separation phenomena in CoNiCuAlCr high entropy alloy containing silver. Materials Science and Engineering: A. 2013;560:633-42.
36. Hsu US, Hung UD, Yeh JW, Chen SK, Huang YS, Yang CC. Alloying behavior of iron, gold and silver in AlCoCrCuNi-based equimolar high-entropy alloys. Materials Science and Engineering: A. 2007;460-461:403-8.
38. Munitz A, Kaufman MJ, Abbaschian R. Liquid phase separation in transition element high entropy alloys. Intermetallics. 2017;86:59-72.

39. Wu PH, Liu N, Yang W, Zhu ZX, Lu YP, Wang XJ. Microstructure and solidification behavior of multicomponent CoCrCu x FeMoNi high-entropy alloys. Materials Science and Engineering: A. 2015;642:142-9.
40. Derimow N, Abbaschian R. Solidification microstructures and calculated mixing enthalpies in CoCrCu containing alloys. Materials Today Communications. 2018;15:1-10.
41. Murty BS, Yeh JW, Ranganathan S. A Brief History of Alloys and the Birth of High-Entropy Alloys. High Entropy Alloys: Elsevier; 2014. p. 1-12.
42. Liu C, Peng W, Jiang CS, Guo H, Tao J, Deng X, Chen Z. Composition and phase structure dependence of mechanical and magnetic properties for AlCoCuFeNi high entropy alloys. Journal of Materials Science & Technology. 2019;35(6):1175-83.
43. Chang X, Zeng M, Liu K, Fu L. Phase Engineering of High-Entropy Alloys. Advanced Materials. 2020;32(14).
44. He MY, Shen YF, Jia N, Liaw PK. C and N doping in high-entropy alloys: A pathway to achieve desired strength-ductility synergy. Applied Materials Today. 2021;25:101162.
45. Mayahi R. A theoretical investigation on deformation behavior and phase prediction of CoCrFeNi-based high entropy alloys. Materials Today Communications. 2020;24:101025.
46. Daryoush S, Mirzadeh H, Ataie A. Advances in the Processing of High-Entropy Alloys by Mechanical Alloying. Advanced Nanomaterials: Springer International Publishing; 2022. p. 531-59.
47. Martin P, Madrid-Cortes CE, Cáceres C, Araya N, Aguilar C, Cabrera JM. HEAPS: A user-friendly tool for the design and exploration of high-entropy alloys based on semi-empirical parameters. Computer Physics Communications. 2022;278:108398.
48. Takeuchi A, Inoue A. Classification of bulk metallic glasses by atomic size difference, heat of mixing and period of constituent elements and its application to characterization of the main alloying element. Materials transactions. 2005;46(12):2817-29.
49. Wang XR, Wang ZQ, He P, Lin TS. The concept, construction and application of mixing enthalpy matrix for high-entropy alloys.
50. Owen LR, Jones NG. Lattice distortions in high-entropy alloys. Journal of Materials Research. 2018;33(19):2954-69.
51. Chen C, Yuan S, Chen J, Wang W, Zhang W, Wei R, et al. A Co-free Cr-Fe-Ni-Al-Si high entropy alloy with outstanding corrosion resistance and high hardness fabricated by laser surface melting. Materials Letters. 2022;314:131882.
52. Du C, Hu L, Pan Q, Chen K, Zhou P, Wang G. Effect of Cu on the strengthening and embrittling of an FeCoNiCr-xCu HEA. Materials Science and Engineering: A. 2022;832:142413.
53. Zhang P, Xu Z, Yao Z, Liu Y, Lin S, He M, et al. A high-corrosion-resistant high-entropy alloys (HEAs) coatings with single BCC solid solution structure by laser remelting. Materials Letters. 2022;324:132728.
54. He Q, Yang Y. On Lattice Distortion in High Entropy Alloys. Frontiers in Materials. 2018;5.
55. Martienssen W. Semiconductors. Springer Handbook of Condensed Matter and Materials Data: Springer Berlin Heidelberg. p. 575-694.
56. Moazzen P, Toroghinejad MR. Enhancement of mechanical properties of a novel single phase Ni1.5FeCrCu0.5 HEA through cold rolling and subsequent annealing. Materials Science and Engineering: A. 2022;848:143360.